Polymer 142 (2018) 375–386

Contents lists available at ScienceDirect

Polymer

journal homepage: www.elsevier.com/locate/polymer

# Interfacial interactions in bicomponent polymer fibers

A. Andrés Leal [a, *, 1], Olivia A. Neururer [a], Alex Bian [b], Ali Gooneie [a], Patrick Rupper [a], Kunal Masania [b, 2], Clemens Dransfeld [b], Rudolf Hufenus [a]

[a] *Laboratory for Advanced Fibers, Empa, Swiss Federal Laboratories for Materials Science and Technology, Lerchenfeldstrasse 5, 9014, St. Gallen, Switzerland*
[b] *Institute of Polymer Engineering, FHNW University of Applied Sciences and Arts Northwestern Switzerland, Klosterzelgstrasse 2, 5210, Windisch, Switzerland*

ARTICLE INFO

*Article history:*
Received 27 January 2018
Received in revised form
23 March 2018
Accepted 26 March 2018
Available online 27 March 2018

*Keywords:*
Thermoplastic
Interface
Fiber

ABSTRACT

The core – sheath interfacial interactions in a bicomponent thermoplastic filament have been analyzed by means of an adapted micro-mechanical approach for interfacial pull-out. The method relies on a specimen preparation procedure that selectively removes a segment of the sheath component while leaving the core intact. This adaptation of the classical pull-out method enables the controlled extraction of the exposed core from the embedded bicomponent segment. Using linear low density polyethylene (LLDPE) – polyamide 6 (PA6) filaments with a diameter of approximately 100 μm, it has been shown that the addition of 2–5 weight % maleic anhydride grafted polyethylene (MAPE) significantly increases the surface energy of LLDPE, which results in substantial improvements in the mean interfacial shear strength and work to debond. Use of 10 % wt. MAPE leads to the formation of voids which are detrimental to the mechanical properties of the core – sheath interface, despite a further enhancement of surface energy.

## 1. Introduction

Multicomponent coextrusion provides the possibility to combine polymers with diverging properties into a composite extrudate, which portrays a new set of attributes that have not been obtained previously. Given that the various material properties of interest are usually found in polymers of dissimilar chemical composition, this provides an implicit motivation to combine relatively incompatible (e.g. immiscible) polymers. In this context, interfacial interactions become extremely relevant and have been a transcendental topic of study [1,2], where the interface between two coextruded polymers displays, within a length scale of a few nanometers [3], composition and energy gradients dictated by the bulk materials that surround it.

Bicomponent fiber spinning can be defined as a particular type of polymer coextrusion in which the extrudate (fiber or filament) has generally a diameter not exceeding 100 μm, where the polymer chains are expressly parallelized to produce highly anisotropic materials. Kikutani et al. [4] have previously shown that structure development of a component is strongly influenced by the elongational viscosity and solidification temperature of the second component during melt spinning of bicomponent fibers. The challenges typically encountered in the compatibilization of immiscible polymer blends [5] also plays a crucial role in bicomponent fiber spinning and are exacerbated by the almost instantaneous solidification induced on the two polymer melts right after they come in contact and exit the spinneret [6]. Hence, the formation of an interfacial adhesion layer will be a function of temperature, molecular weight, polydispersity, chain orientation, and molecular structure of the polymers [7,8], among others. Attempts to enhance the interfacial interactions between components in melt-spun materials have prompted for instance to the development by Southern et al. [9] of a modified spin-unit pack-assembly that guides the bicomponent molten stream through porous media, forcing the formation of a highly irregular interface. As a result, the adhesion between the core and sheath components is enhanced by means of a mechanical interlocking of the two constituents. Atomic force microscopy of several fiber types has shown the self-affinity of their surface roughness over a number of scales, demonstrating a fractal nature of fiber surfaces which extends to the

---

* Corresponding author.
*E-mail address:* andres.leal-ayala@ch.abb.com (A.A. Leal).
[1] Present address: Insulation and Polymer Technologies Group, Energy and Materials Department, Corporate Research, ABB Switzerland Ltd., Segelhofstrasse 1 K, 5405 Baden, Switzerland.
[2] Present address: Complex Materials Group, Department of Materials, ETH Zurich, 8093 Zurich, Switzerland.

https://doi.org/10.1016/j.polymer.2018.03.055

interfaces formed by them [10]. Dasdemir et al. [11] have analyzed the polymer-polymer compatibility for material systems used in their study to spin bicomponent fibers, finding a direct relation between core-sheath interfacial affinity and fiber tensile properties. The addition of polypropylene grafted with maleic anhydride (MA) to a polypropylene (PP) – polyethylene terephthalate (PET) bicomponent fiber led to a significant improvement in tensile strength which was attributed to the MA acting as an interfacial emulsifying agent [12], with similar results reported when using MA-grafted PP as an additive for the development of PP sheath – polyamide 6 (PA6) core filaments [13]. Ide and Hasegawa have explained how the presence of MA-grafted PP enhances the compatibility of PP-PA6 polymer blends due to the formation of a grafted polymer between the MA in PP and the amine functional groups of PA6, where the mechanical properties of the blend are significantly enhanced as a function of the amount of MA added to it [14].

Interest to better understand the nature of fiber-matrix interfaces has fostered the development of micro-mechanical techniques, which allow the quantification of interfacial interactions. Making use of model composite systems (i.e. a single filament partially embedded in a matrix), parameters such as interfacial shear strength and work to debond can be determined [15,16]. The choice of micro-mechanical technique that better fits a particular material system is a function of diverse fiber properties such as brittleness, elongation to break and tendency to fibrillate; and geometric characteristics such as fiber diameter and critical fiber length to debond. Thus, in the case of the bicomponent melt-spun filaments that have been studied in the present work, the single fiber pull-out test has been selected to probe the mechanical behavior of the core-sheath interface. Various authors have analyzed the behavior of the fiber-matrix interface during fiber pull-out [17–19]. The load-displacement curve begins with a linear elastic region which reflects the ability of the interface to accommodate the applied load. This is followed by a decline on the slope of the load-displacement curve, indicating the onset of plastic deformation which could be caused by matrix yielding in the vicinity of the interface, interfacial debonding coupled with crack propagation, or a combination of both phenomena. Once crack propagation becomes unstable and the remaining interface is completely detached, the load-displacement curve shows a sharp decrease which is followed by a low force level associated with frictional forces generated as the fiber slides out of the matrix. The single fiber pull-out test has been successfully employed to quantify the effect of MA-grafted polymers on the properties of the interfaces formed between carbon fibers and thermoplastics. Accordingly, Tran et al. were able to measure a 180% improvement in interfacial shear strength when MA-grafted poly(vinylidene fluoride) (PVDF) was added to PVDF [20], while Li and Sun observed a similar behavior when polystyrene (PS) was enhanced with MA-grafted PS [21]. Nevertheless, to the best of our knowledge, a direct quantification of the mechanical characteristics at a fully-thermoplastic core – sheath interface has never been reported and is therefore the present goal. Given that the characteristics of the interface influence the mechanical performance of the bicomponent fiber as a whole, a thorough understanding of the mechanical performance at the interface will allow, first, to better predict, and then, to tailor and fine-tune the behavior of the fiber during service.

The current work describes a newly developed micro-mechanical technique to probe the interfacial affinity between the core and sheath constituents of a melt-spun bicomponent filament. The method, based on a modification of the pull-out technique, quantifies the force needed to detach and extract the fiber core from the sheath component, allowing the calculation of interfacial shear strength between a core and sheath, for the first time. The interfacial affinity between linear low density polyethylene (LLDPE) and PA6 in a filament having a diameter in the order of 100 μm is investigated. The effect of adding maleic anhydride grafted polyethylene (MAPE) to the LLDPE component on the compatibilization of the PE – PA interface is analyzed by thermal analysis, rheology, surface energy determination and interfacial pull-out tests.

## 2. Materials and methods

### 2.1. Materials

Commercially available polymers were used to produce core-sheath bicomponent monofilaments: Grilon F 34 NL (PA6) from EMS-GRIVORY, Dowlex SC 2108G (LLDPE) from The Dow Chemical Company, and Licocene 4351 maleic anhydride grafted polyethylene (MAPE) from Clariant, as shown by their chemical structures illustrated in Fig. 1.

### 2.2. Thermal, rheological and surface characteristics

Thermal, rheological and surface analyses have been performed, with a particular emphasis on the behavior of MAPE, PA6 and LLDPE at 260 °C, which is the spinneret temperature used for fiber melt

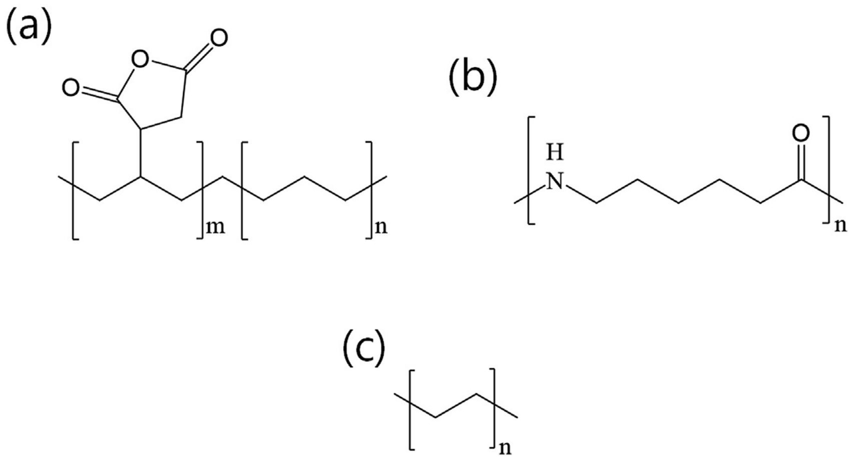

**Fig. 1.** Chemical structures of (a) MAPE, (b) PA6 and (c) LLDPE.

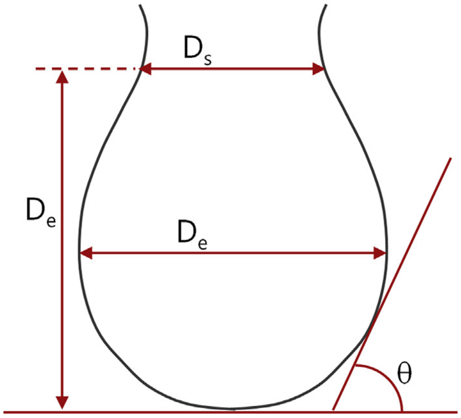

**Fig. 2.** Geometry of the pendant drop shapes that were studied [25].

**Table 1**
Composition of the bicomponent filaments under analysis.

| Fiber type | Core | Sheath |
|---|---|---|
| LLDPE – PA6 | LLDPE + x % MAPE[a] | PA6 |
| PA6 – LLDPE | PA6 | LLDPE + x % MAPE[a] |

[a] x = 0, 1, 2, 5 or 10 weight percent.

spinning. Differential scanning calorimetry (DSC) was performed on a TA DSC Q 1000 from TA Instruments with heating and cooling rates of 10 °C/min under a nitrogen atmosphere, where the 4–7 mg specimens were subjected to two sets of heating and cooling cycles: from 0 to 300 °C for PA6 and LLDPE, and from 0 to 200 °C for MAPE. Thermogravimetric analysis (TGA) of MAPE was carried out using a TGA Q500 from TA Instruments, where 32–35 mg of material where analyzed under a nitrogen atmosphere. Two different temperature ramps were employed for TGA: 25–350 °C with a heating rate of 10 °C/min, and 25–260 °C with a heating rate of 40 °C/min followed by an isotherm at 260 °C during 1 h. Rheological measurements were performed to determine the zero-shear viscosity ($\eta_0$) of the polymers at 260 °C. The steady shear flow experiments were conducted at a constant shear rate of 0.1 $s^{-1}$. This shear rate has been shown before to fall well within the Newtonian region of the flow curve of various polymer melts and is therefore appropriate to estimate the zero-shear viscosity value [22,23]. The rheological measurements were performed using a rheometric mechanical spectrometer (Anton Paar Physica MCR 301). All measurements were done in a nitrogen environment utilizing a parallel plate fixture with a diameter of 25 mm and a constant gap of 1 mm. In order to minimize the influence of processing history, all samples were held at the testing temperature for 25 min in the nitrogen environment prior to the measurement. The steady state viscosity was averaged over time for 150 s and taken as the zero-shear viscosity of the samples.

The surface energy of the molten polymers at 260 °C was determined following the pendant drop method [24] under a nitrogen atmosphere, using a Drop Shape Analyzer DSA100 from Krüss, equipped with an environmental chamber and a high temperature dosing system DO3241 with a calibrated 2 mm tip. Samples of each polymer were melted until a hanging droplet was formed at the tip of the dosing system. Three droplets of each polymer were analyzed, where the shape measurement of each droplet was performed once per second, and the lowest measured value was taken as the surface energy of the polymer. Care was taken to perform the measurements within the first 5 min of each experiment to ensure that the data were not influenced by thermal degradation or transient effects of the polymer melts. The pendant drop method involves the calculation of the surface energy via a derivation of the Young Laplace equation. This equation describes the pressure difference between two static fluids – in this case, polymer and nitrogen gas – due to the surface tension of the molten polymer. Hansen and Rodsrud [25] derive an expression of surface tension ($\gamma$) from the Young Laplace equation as:

$$\gamma = \frac{\Delta\rho g R_o^2}{\beta} \tag{1}$$

where $\Delta\rho$ represents the pressure difference across the polymer – surrounding medium interface, g is the gravitational constant, $R_o$ is the radius of curvature at the drop apex, and $\beta$ denotes the shape factor as defined in Equation (2) [25], with $\sigma$ defined as the ratio $D_s/D_e$ (Fig. 2).

$$\beta = 0.12836 - 0.7577\sigma + 1.7713\sigma^2 - 0.5426\sigma^3 \tag{2}$$

### 2.3. Melt spinning of core-sheath bicomponent fibers

The bicomponent monofilaments were melt spun on Empa's pilot plant described previously in Ref. [26]. Before melt spinning, PA6 was dried in a vacuum oven for 8 h at 100 °C, while LLDPE and the LLDPE-MAPE mixtures were dried in the vacuum oven at 60 °C for 8 h. PA6 was processed with an 18 mm single screw extruder having a length-to-diameter (L/D) ratio of 25, while LLDPE and the LLDPE-MAPE mixtures were processed with a 13 mm single screw extruder which also has an L/D ratio of 25. Static mixers with eight mixing elements were coupled to both extruders to homogenize each polymer melt. The bicomponent spinneret consists of a bore of

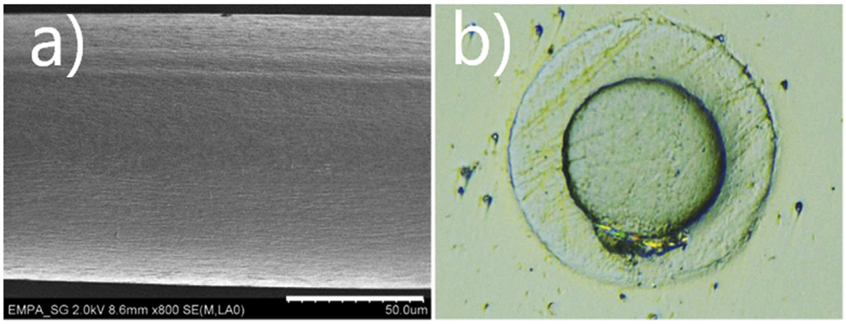

**Fig. 3.** (A) Scanning electron micrograph of longitudinal view of PA6-LLDPE core-sheath and (b) optical micrograph of cross sectional view of LLDPE-PA6 core-sheath bicomponent filaments under analysis.

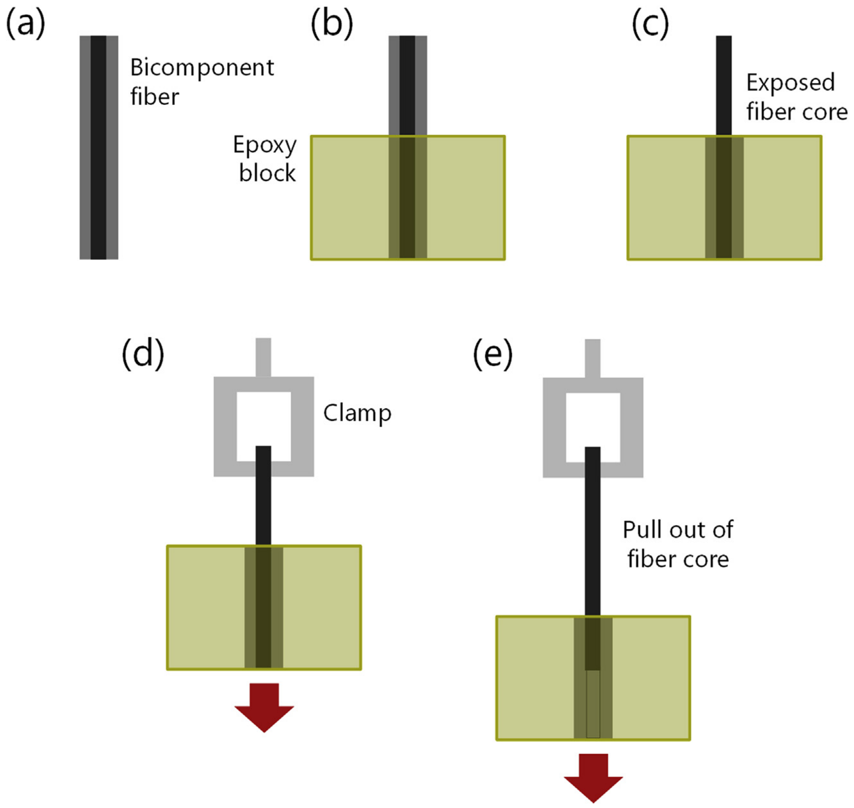

**Fig. 4.** Specimen preparation and pull-out testing: (a) core-sheath bicomponent filament, (b) embedding in an epoxy block, (c) removal of fiber sheath on free end of fiber, (d) mounting in universal testing machine and (e) core-sheath pull-out testing.

**Table 2**
Procedures to chemically remove the fiber sheaths.

| | LLDPE sheath | PA6 sheath |
|---|---|---|
| Solvent | Hot toluene (100 °C), stirred | Formic acid, stirred |
| Time to full sheath dissolution | 27 min | 1 min |
| Washing | With deionized water | |

1.2 mm in which a capillary with an inner diameter of 0.6 mm and a wall thickness of 0.15 mm is placed concentrically, enabling the spinning of a monofilament with a core-sheath configuration. This type of spinneret, called multiple die spinneret, enables the extrusion of each polymer separately, where both materials only come in contact at the end of the capillary, reducing rheological disparities [7]. Melt spinning was performed at a spinneret temperature of 260 °C. Drawing of the monofilament was performed immediately after spinning by means of three godets using a draw ratio of 3.5 (draw ratio = speed of godet 3/speed of godet 1), where the winding speed of the drawn filament was 1050 m/min. The diameter of the produced filaments was in the order of 100 µm with a core/sheath volumetric ratio of 1:1. A description of the bicomponent filaments melt spun for this work is presented in Table 1, while Fig. 3 shows longitudinal and cross sectional views of the resulting filaments.

### 2.4. Microscopy

The morphology of the original bicomponent filaments and of the tested specimens was analyzed using scanning electron microscopy (SEM). Specimens were fixed on a holder with carbon tape and sputter coated to apply a 5 nm gold/palladium film with the high vacuum deposition system Leica EM ACE600. The coated specimens were then scanned using a Hitachi S-4800 field emission SEM with accelerating voltages of 2.0 kV or 20 kV and an emission current of 10 µA. Optical microscopy pictures were taken using a Keyence VHX-1000 system.

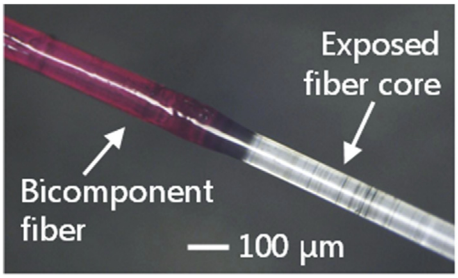

**Fig. 5.** Dyed LLDPE-PA6 core-sheath bicomponent filament which has been partially immersed in formic acid to chemically remove the dyed polyamide sheath (fiber diameter: 96 µm; diameter of exposed core: 77 µm).

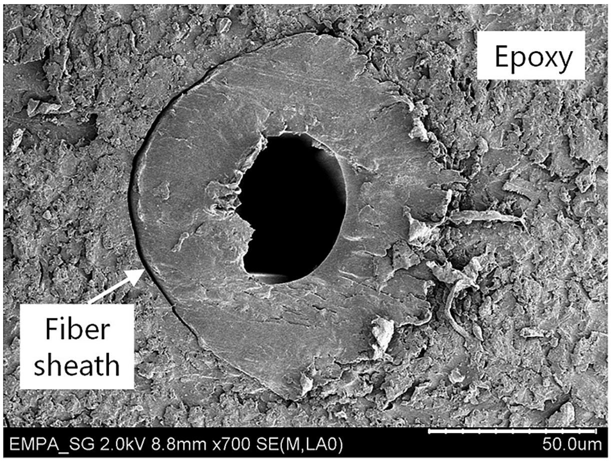

**Fig. 6.** SEM micrograph of the bottom side of a specimen after core-sheath pull-out testing. The successful pull-out of the LLDPE fiber core from the PA6 sheath can be clearly observed.

### 2.5. *Mechanical properties of core-sheath interface*

The single fiber pull-out test, a micro-mechanical experimental method typically used to evaluate the interfacial properties of fiber-matrix systems in fiber-reinforced composites [27,28], has been modified in this work to quantify the interfacial interactions between the core and sheath components of a bicomponent fiber. Fig. 4 illustrates schematically the procedure employed to prepare a specimen suitable for core-sheath pull-out testing: A bicomponent filament is embedded in epoxy resin. Once the epoxy has cured, the sheath of the protruding fiber end is chemically dissolved to expose the fiber core. The details of the dissolution procedures used to chemically remove the fiber sheaths are summarized in Table 2. The solvent selected in each case dissolves the sheath material efficiently without attacking the corresponding core polymer. The epoxy block is sliced perpendicularly to the fiber direction to reduce the length of embedded fiber to approximately 5 mm. This guarantees that failure is the result of core-sheath interfacial detachment within the block, avoiding tensile fracture of the core component outside the embedded region. The epoxy block and the

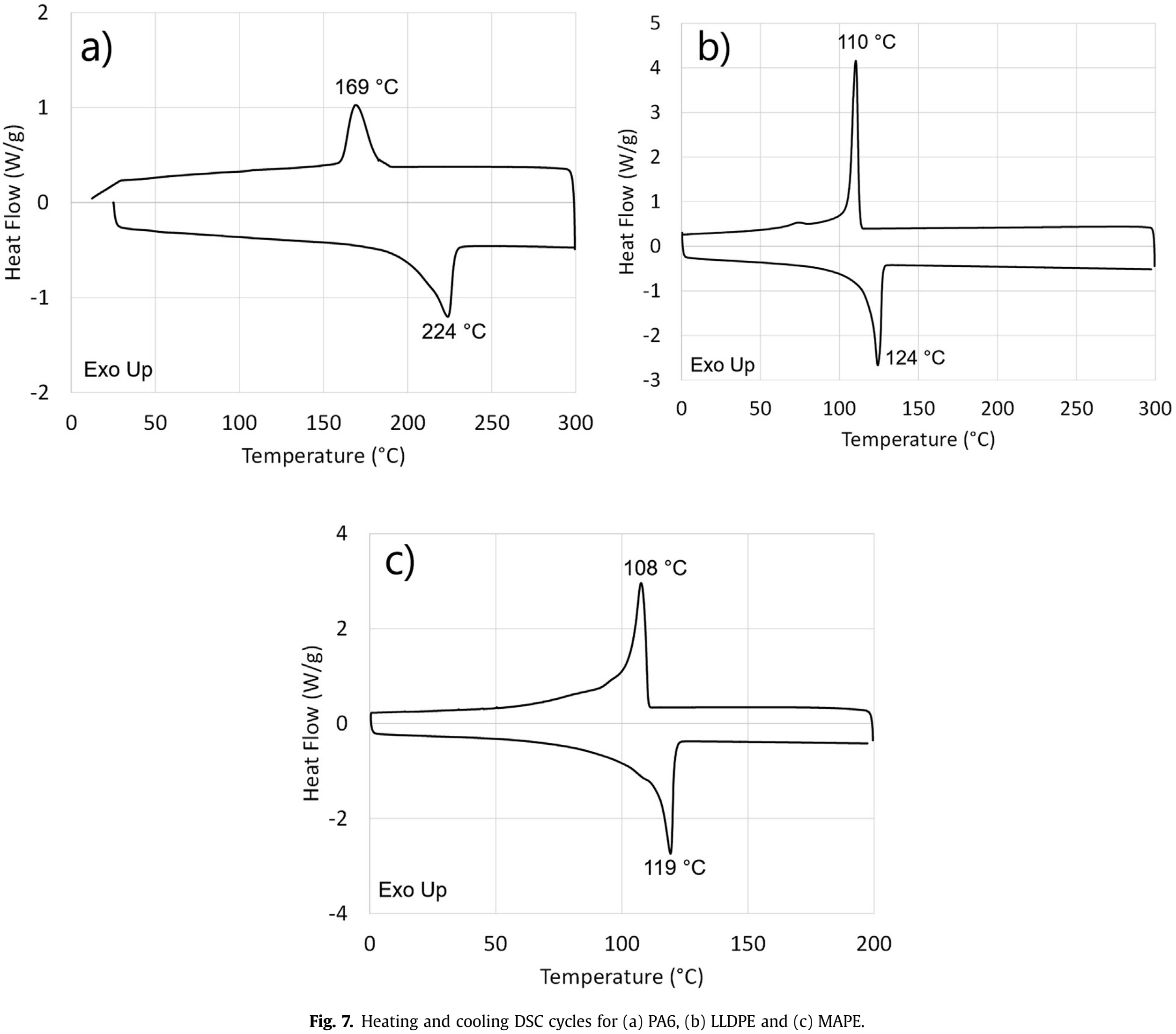

**Fig. 7.** Heating and cooling DSC cycles for (a) PA6, (b) LLDPE and (c) MAPE.

protruding fiber core are clamped in a universal testing machine and the force required to detach the core from the sheath at a constant rate of extension is measured.

Full sheath dissolution was verified by optical microscopy and the property retention of the exposed core was confirmed by means of mechanical testing, where the tensile properties of filament cores remained unchanged before and after immersion in the solvent in question. Fig. 5 shows a bicomponent filament where the polyamide sheath was first dyed with an acid dye, and then the right side of the bicomponent fiber was subjected to the dissolution procedure. The image illustrates that the PA6 sheath was fully removed, with a neat transition region having a length of about 100 μm (about 2% of the total embedded length) between treated and untreated regions. The dissolution procedure has proven to be repeatable and thus significant variations in the length of the bicomponent – core transition region were not detected.

The core-sheath pull-out tests were performed with a 10 N load cell mounted on a Zwick Z100 universal testing machine using a clamping length of 10 mm and a rate of extension of 5 mm/min. Sixteen specimens were tested for each fiber type. The successful pull-out of each fiber core was confirmed by optical and scanning electron microscopy. A micrograph of the bottom side of a tested specimen is presented in Fig. 6, where the PA6 sheath and the surrounding epoxy are clearly observed along with the cavity left behind by the pulled-out core. In the case of the LLDPE sheath specimens, the adhesion between LLDPE and epoxy was enhanced by means of a plasma treatment applied to the surface of the filament before embedding it in epoxy as detailed in Ref. [29]. Without this treatment, the interfacial shear strength between PA6 and LLDPE was higher than between LLDPE and epoxy, impeding pull-out of the core.

### 2.6. Chemical composition

Attenuated total reflection Fourier transform infrared spectroscopy (ATR-FTIR) has been employed to confirm the existence of MA in the LLDPE-MAPE extruded blends. FTIR spectra were acquired with a Varian 640-IR spectrometer recording 32 scans at a resolution of 4 $cm^{-1}$. Energy-dispersive X-ray spectroscopy (EDX) was used to analyze the surface composition of pulled-out cores. For this purpose, an Inca X-sight EDX system was used in combination with the Hitachi S-4800 SEM described above. Point measurements with a depth of penetration in the order of 1–3 μm were performed using an acceleration voltage of the electron beam of 20 kV, an emission current of 10 μA and a working distance of 15 mm.

## 3. Results

### 3.1. Thermal properties of starting materials

DSC scans showing cooling and second heating cycles for the starting polymers are illustrated in Fig. 7. The measured melting temperatures are 224 °C for PA6, 127 °C for LLDPE (second heating) and 119 °C for MAPE (second heating). Based on melt spinning preliminary trials, a spinneret temperature of 260 °C was selected as the optimal processing temperature for this material system. The TGA scan of MAPE (Fig. 8a) indicates that at 260 °C, MAPE has suffered a weight reduction of less than 4%. Likewise, a TGA isotherm at 260 °C (Fig. 8b) revealed weight loss of less than 2% after 6 min, and less than 9% after 60 min. Therefore, MAPE does not appear to suffer substantial thermal degradation as a result of the melt spinning process.

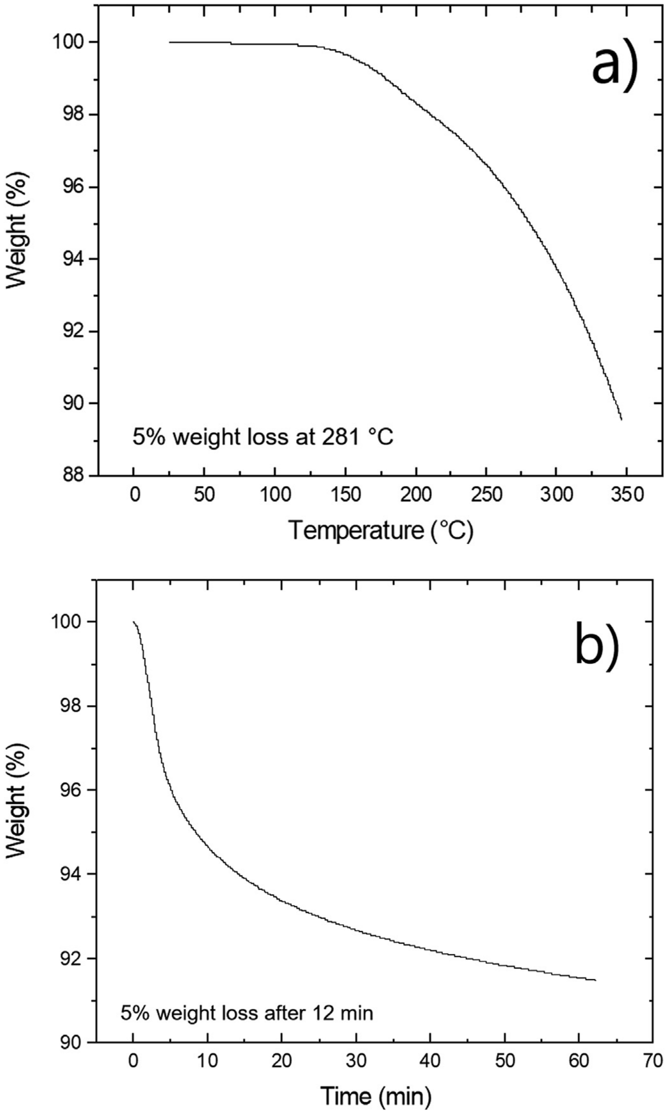

**Fig. 8.** TGA of MAPE: (a) heating rate of 10 °C/min, and (b) 260 °C isotherm.

### 3.2. Surface energy and rheological properties of polymer melts

The measured values of surface energy in Fig. 9a show that the addition of MAPE to LLDPE results in significant differences: as the % MAPE increases, so does the surface energy of the LLDPE + MAPE blend. The addition of 10% MAPE increases the surface energy of the PE blend by 24%. Clearly, the use of melt blender static mixers during fiber spinning has allowed to produce homogeneous MAPE –LLDPE blends. The surface energy value for LLDPE obtained in the present work correlates well with the measurements performed by Moreira and Demarquette [30], who reported a value of 20.2 mN/m for LLDPE at 260 °C, using the pendant drop method. However, the addition of MAPE also influences the rheology of the PE blends, as found in the case of their zero-shear viscosities (Fig. 9b). Analogous to the surface energy measurements, the value of $\eta_0$ increases steadily with % MAPE added. The maleic anhydride moiety is clearly perturbing the flow behavior of the LLDPE, to the extent where 10% added MAPE increases $\eta_0$ by 26%. If the observed increase in viscosity mismatch between LLDPE and PA6 as % MAPE is increased can be extrapolated to higher shear rates, the enhancement in surface energy of

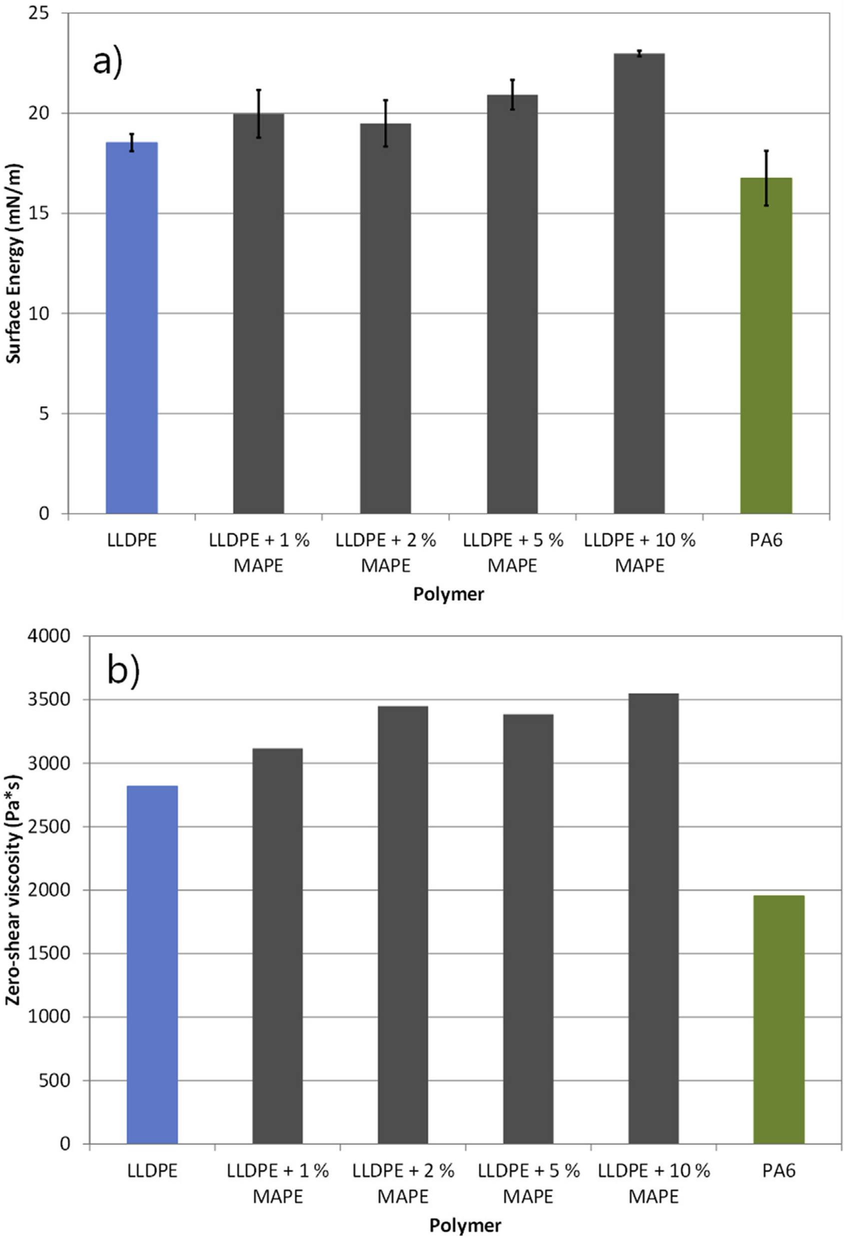

**Fig. 9.** (A) Surface energies and (b) zero-shear viscosities for the different polymers and polymer blends under analysis. The error bars represent ± one standard deviation. The repeatability of the $\eta_0$ measurements was extremely high and no significant variability can be observed. All measurements were performed at 260 °C.

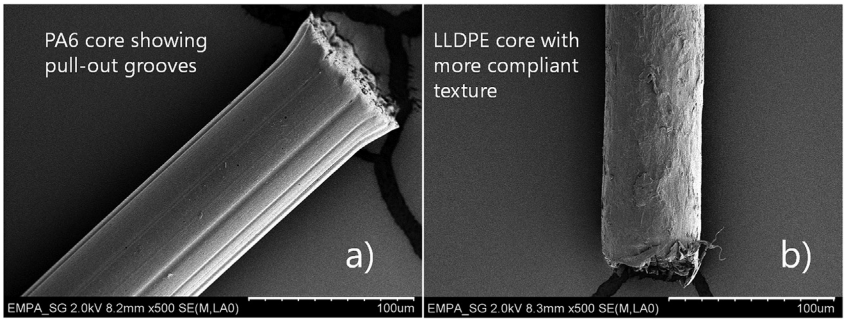

**Fig. 10.** Examples of pulled-out (a) PA6 and (b) LLDPE cores.

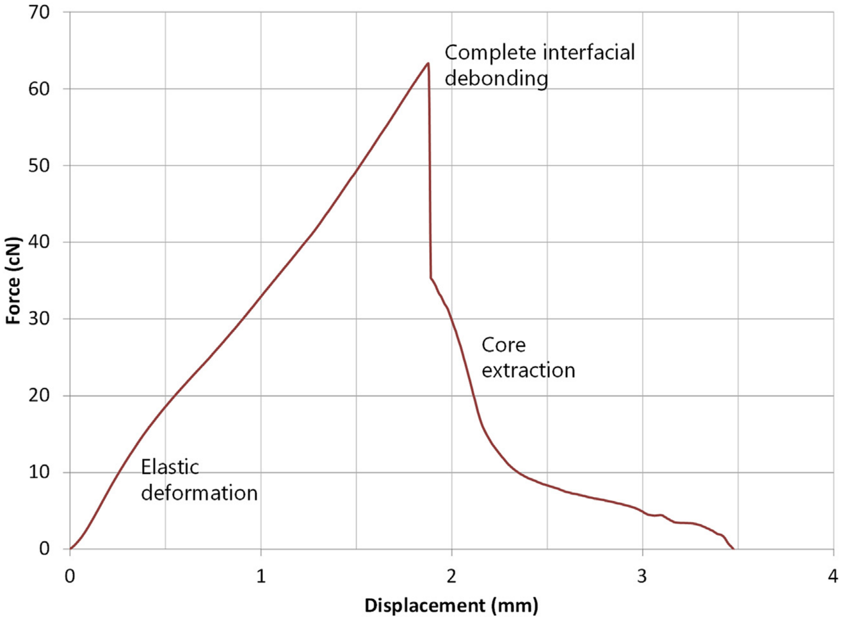

**Fig. 11.** Typical load – displacement plot from a single fiber pull-out test for a PA6 core/LLDPE sheath specimen.

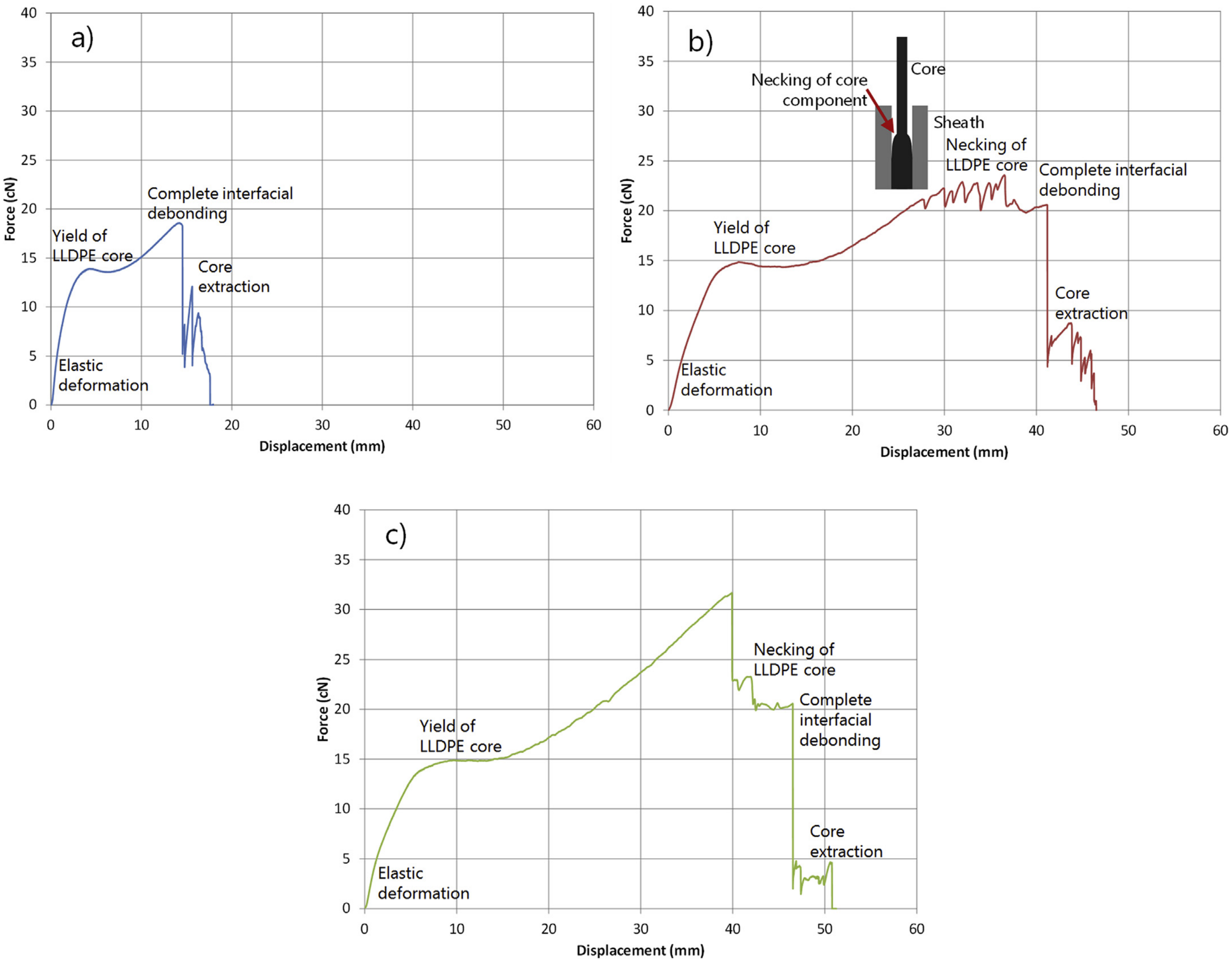

**Fig. 12.** Load – displacement plots from a single fiber pull-out test for LLDPE core/PA6 sheath specimens for LLDPE (a) without MAPE, (b) with 1% MAPE, and (c) with 2% MAPE.

the PE blends is obtained at the expense of a reduction in processability of the PE – PA6 material system. An exacerbation of the viscosity mismatch may preclude the full draw-off of the less viscous material, as the drawing off process will be limited by the drawability of the more viscous component [31].

### 3.3. Mechanical properties of core-sheath interface

#### 3.3.1. Pull-out mechanism

SEM micrographs of pulled out PA6 and LLDPE cores are presented in Fig. 10. The PA6 core exhibits what seem to be distinct pull-out grooves, while the LLDPE core appears to have a more compliant texture. Fig. 11 shows a typical load – displacement curve for a pull-out of a PA6 core. The displacement range between 0.15 mm and 0.35 mm depicts a region of purely elastic deformation of the core. This is followed by a convex bend of the curve that could be associated with partial yielding and limited strain hardening of the ductile LLDPE sheath, since it is known that radial and circumferential stresses are effected not only at the interface, but also in the matrix (sheath) region immediately adjacent to the interface [32]. The linear behavior is then resumed for the displacement range between 0.75 and 1.25 mm. Then the slope becomes slightly steeper and remains constant as the interface is linearly loaded [18]. The point of complete interfacial debonding is ultimately reached at a displacement of 1.9 mm. A drastic drop in the measured force right after debonding and the subsequent extraction of the detached core compose the final segments of the plot. The fact that the extraction of the detached core occurs in a gradual, controlled manner is characteristic of relatively weakly bonded interfaces [27].

In contrast, the LLDPE cores display a completely different pull-out behavior which is analogous to the debonding mechanism reported by Bowling and Groves for the pull-out of ductile wires [33]. The presence of MA in the pulled-out LLDPE + MAPE cores has been confirmed by means of ATR-FTIR, where the spectroscopic analysis indicates the existence of typical MA bands such as ring structure carbonyl asymmetric and symmetric stretches around 1830 $cm^{-1}$ and 1780 $cm^{-1}$ and a C=O carboxyl stretching band at 1720 $cm^{-1}$, respectively [34,35]. Load – displacement curves for LLDPE cores containing different amounts of MAPE are shown in Fig. 12. All three pull-out plots display an initial zone with a very steep slope indicative of elastic deformation. The slope becomes gradually shallower as the core partially debonds. Once the applied force reaches a value of approximately 15 cN, the core segments that have already been debonded undergo tensile yielding. This is followed by a state of mixed deformation: crack propagation at the interface, and plastic deformation with possible strain hardening of the debonded core. Then, depending on the strength of the interface, three possible outcomes are observed. For a very weak interface (Fig. 12a, LLDPE core without MAPE), complete interfacial debonding is achieved before the applied force reaches 20 cN, at a displacement of 15 mm. When 1% MAPE is added to the LLDPE core (Fig. 12b), plastic deformation and interfacial debonding withstand forces in excess of 20 cN. Once the length of debonded core reaches a critical value, the pull-out plot portrays a region of instability, in the displacement range between 28 mm and 40 mm (Fig. 12b). This instability is caused by neck formation and propagation within the debonded core segment. Evidence of neck formation and propagation within this region has been found on the pulled-out LLDPE + MAPE cores, as illustrated in Fig. 13. LLDPE's propensity to neck formation is due to its incomplete drawing during the bicomponent fiber drawing-off process, which is controlled by the PA6 component. Having a higher melting temperature, PA6 solidifies first and inhibits LLDPE's full drawing [4,7]. The fact that the necking happens only within the debonded core segment and not on the exposed fiber core (Fig. 4c) indicates that this deformation may be the result of a higher stress level induced either by the radial and circumferential stresses at the remaining interface, or by the frictional forces acting on the freshly debonded core segment. The necking stage in the load – displacement curve of Fig. 12b precedes a final stage of interfacial debonding in the displacement range between 40 mm and 42 mm, resulting in full core-sheath detachment and abrupt force reduction. In the case where 2% MAPE was added to the LLDPE core (Fig. 12c), the core-sheath interfacial interactions have been successfully enhanced in such a way, that an applied force in the order of 32 cN is reached before the debonded core segment attains the critical length to initiate the necking deformation. Neck formation and propagation also takes place at a force level of 20 cN–25 cN as in the case of the LLDPE core with 1% MAPE (Fig. 12b). The load – displacement plots presented in Fig. 12 clearly indicate an enhancement of interfacial interactions as MAPE is added to LLDPE.

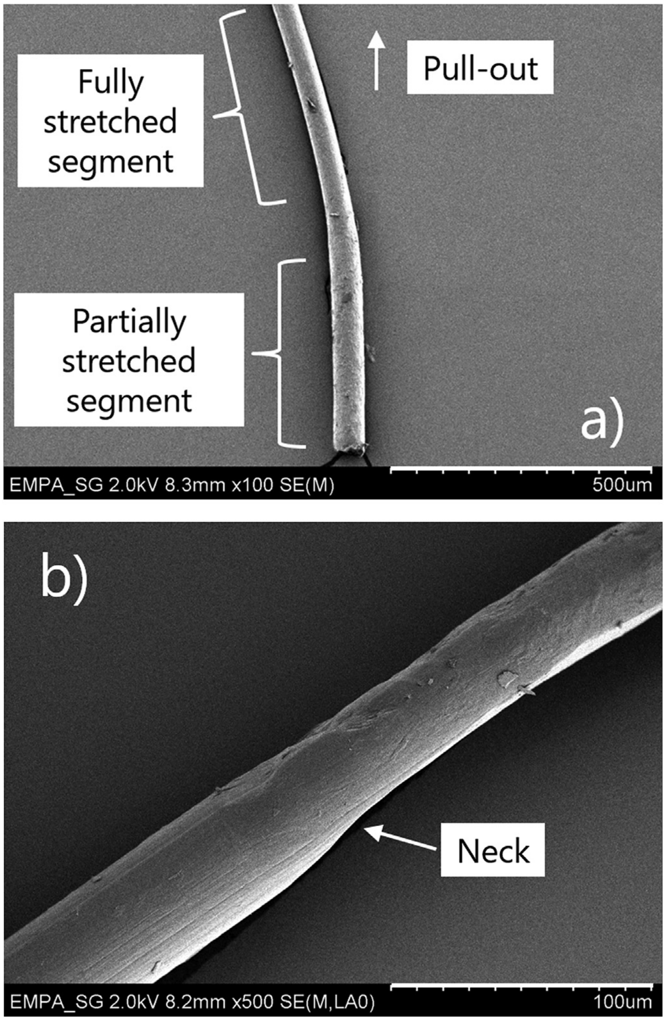

**Fig. 13.** LLDPE cores exhibiting (a) fully and partially stretched segments due to neck formation and propagation during pull-out, and (b) detail of necking deformation.

#### 3.3.2. Interfacial shear strength and work to debond

The maximum force values ($F_{max}$) were used to calculate mean interfacial shear strength (IFSS) values according to Equation (3) [36]:

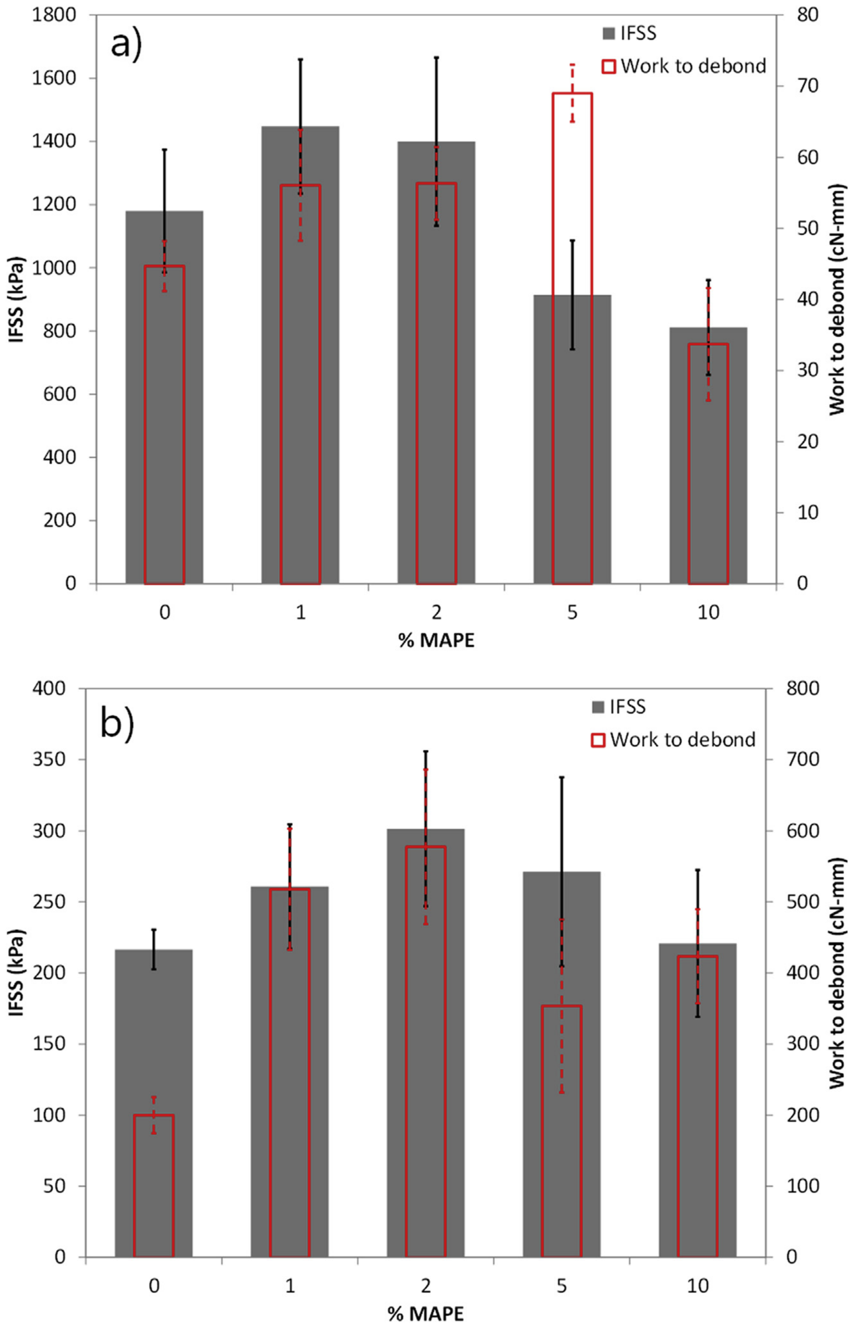

**Fig. 14.** Average interfacial shear strength and work to debond from the pull-out experiments of (a) PA6 and (b) LLDPE cores as a function of weight % MAPE added to the LLDPE component. The error bars represent ± one standard deviation.

$$IFSS = \frac{F_{max}}{2\pi r l} \qquad (3)$$

where r and l in Equation (3) represent core radius and pull-out length, respectively. Specimens were prepared so that the pull-out lengths were approximately 5 mm in all cases. The purpose of this was to maintain a constant shear stress distribution and hence avoid any effects on the debonding phenomena. The measured IFSS are summarized in Fig. 14 along with the “work to debond” – the area under the load – displacement curves resulting from the core-sheath pull-outs. With respect to the PA6 cores (Fig. 14a), the addition of 1–2% MAPE to the LLDPE sheath results in a 23% increase in IFSS with respect to the bicomponent fiber without MAPE, while the addition of 5% MAPE leads to a strong deterioration of the property, reaching an IFSS value lower than that of the original material. In contrast, the work required to detach the PA6 core increases steadily with the addition of MAPE, showing a maximum improvement of 53% when 5% MAPE is added. The increased work needed to detach the core at a lower IFSS may be due to enhanced energy dissipation during frictional sliding of the already detached core segment, as observed by Warren and Krajcinovic, who have reported on the toughening of fiber-matrix interfaces when a fractal interface is present, where the fiber features a self-affinity of its surface morphology which spans from the nano-to the micro-scales [37]. The incorporation of 10% MAPE to

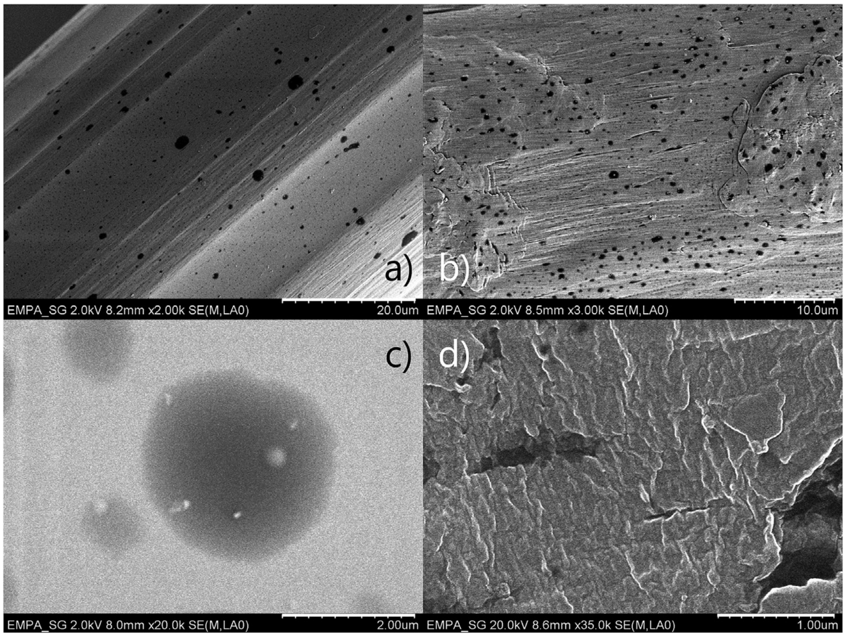

**Fig. 15.** SEM images of (a) PA6 and (b) LLDPE extracted cores where 10% MAPE was incorporated to the LLDPE component, and detailed views of the dark features encountered in the (c) PA6 and (d) LLDPE cores.

the LLDPE sheath is clearly counterproductive, since both IFSS and work to debond are at this stage significantly worse than the values from the reference bicomponent fiber. This is in spite of the fact that the addition of 10% MAPE to LLDPE leads to a 24% increase of its surface energy (Fig. 9a), which would be expected to significantly enhance the PA6 – LLDPE adhesive characteristics. Similar trends, although with different magnitudes, are found in the case of the pull-out of LLDPE cores (Fig. 14b). Addition of 2% MAPE to the LLDPE cores leads to a 40% improvement in IFSS and a 190% increase of the work needed to debond the interface, while both properties deteriorate when 5 or 10% MAPE was used. On top of the expected enhancement in interfacial properties, the incorporation of MA also dramatically increases the ductility of LLDPE.

Analyzing the morphology of the extracted cores from the specimens containing 10% MAPE, both core materials were found to exhibit black features on their surface (Fig. 15a and b). Higher magnification SEM micrographs reveal that, particularly for the LLDPE cores, the observed features represent voids which were formed at the interface of the bicomponent filaments with 10% MAPE (Fig. 15c and d). The chemical composition of the LLDPE +10% MAPE core surfaces were studied using EDX. The investigation indicated no change in chemical composition when focusing on the voids or on the surrounding undamaged surface, measuring a mass % distribution of 91% carbon and 9% oxygen in both cases, confirming that the features represent voids or pores and not a chemically-distinct spot. The formation of voids at the interface of a core-sheath liquid-crystal-polymer (LCP) – PET bicomponent fiber has been reported by Perepelkin [38]. They attributed the formation of such voids to the formation of expanding gas bubbles at the core-sheath interface produced by degassing products of LCP. In the present work, the formation of voids appears to be linked to an excess of MA present at the PA6 – LLDPE interface, although the detailed mechanism of void formation will require further investigation. Nevertheless, it is reasonable to consider that the observed voids serve as weak spots that promote the initiation and propagation of cracks which could lead to a premature failure of the interface during pull-out.

## 4. Conclusions

The pull-out mechanism appears to depend strongly not only on the characteristics of the interface, but also on the processing history of the bulk core and sheath polymers. Therefore, in the case where PA6 is the core material, the general shape of the load – displacement curve remains constant, where the use of the MAPE – LLDPE blends does enhance the maximum pull-out force and work to debond. The draw ratio of 3.5 applied to the bicomponent filament promotes sufficient parallelization of the polymer chains in PA6 for it to survive the pull-out process without further plastic deformation. In contrast, the use of LLDPE as core component produces pull-out mechanisms which are strongly dependent on the amount of MAPE added to the blend. While the use of pure LLDPE leads to a failure behavior in which tensile yielding and plastic deformation of debonded core segments is followed by complete interfacial debonding, the addition of MAPE strengthens the interfacial shear strength to the point where the debonded segments of LLDPE + MAPE blends undergo necking deformation before complete interfacial debonding is achieved. As a result, the maximum IFSS achieved by the PA6 core exceeded 1400 kPa, while the LLDPE core was only able to reach shear strength values in the order of 300 kPa. This phenomenon highlights the importance of choosing polymer pairs for bicomponent melt spinning which have rheological properties (e.g. similar surface energies and viscosities) that will make them a compatible material system.

## Acknowledgements

Clariant is acknowledged for supplying the MAPE used in this work. Benno Wüst is acknowledged for performing the fiber melt-spinning. Marcel Halbeisen is acknowledged for his support in developing the specimen preparation technique for the core – sheath pull-out test. Seraina Bokanyi, Joel Gächter, Pierrine Zeller and Lukas Kurz are acknowledged for preparing the specimens for pull-out testing. Funding: This work was partially supported by the Commission for Technology and Innovation (CTI)of the Swiss

Federal Administration [grant number 13295.1 PFFLR-IW]. K. Masania acknowledges the support of the ETH Foundation grant SP-MaP 01-15; C. Dransfeld and K. Masania acknowledge the support within the framework of the Swiss Competence Center for Energy Research – Efficient Technologies and Systems for Mobility.

## References

[1] B.D. Favis, Polymer alloys and blends - recent advances, Can. J. Chem. Eng. 69 (3) (1991) 619–625.
[2] C.D. Han, Study of bicomponent coextrusion of molten polymers, J. Appl. Polym. Sci. 17 (4) (1973) 1289–1303.
[3] T.P. Russell, A. Menelle, W.A. Hamilton, G.S. Smith, S.K. Satija, C.F. Majkrzak, Width of homopolymer interfaces in the presence of symmetrical diblock copolymers, Macromolecules 24 (20) (1991) 5721–5726.
[4] T. Kikutani, J. Radhakrishnan, S. Arikawa, A. Takaku, N. Okui, X. Jin, F. Niwa, Y. Kudo, High-speed melt spinning of bicomponent fibers: mechanism of fiber structure development in poly(ethylene terephthalate)/polypropylene system, J. Appl. Polym. Sci. 62 (11) (1996) 1913–1924.
[5] L. Robeson, Historical perspective of advances in the science and Technology of polymer blends, Polymers 6 (5) (2014) 1251–1265.
[6] J.E. Spruiell, J.L. White, Structure development during polymer processing - studies of melt spinning of polyethylene and polypropylene fibers, Polym. Eng. Sci. 15 (9) (1975) 660–667.
[7] R. Hufenus, Y. Yan, M. Dauner, D. Yao, T. Kikutani, Bicomponent fibers, in: Jinlian Hu (Ed.), Handbook of Fibrous Materials, Wiley-VCH Publishing Ltd, 2017.
[8] E.L. Jablonski, Interdiffusion Phenomena at Partially Miscible Polymer Interfaces, Iowa State University, 2002.
[9] J.H. Southern, D.H. Martin, D.G. Baird, Improved sheath-core adhesion in biconstituent fibers via interface mixing, Textil. Res. J. 50 (7) (1980) 411–416.
[10] Y.A. Dzenis, D.H. Reneker, V.V. Tsukruk, R. Patil, Fractal analysis of surfaces of advanced reinforcing fibers by atomic force microscopy, Compos. Interfac. 2 (4) (1994) 307–319.
[11] M. Dasdemir, B. Maze, N. Anantharamaiah, B. Pourdeyhimi, Influence of polymer type, composition, and interface on the structural and mechanical properties of core/sheath type bicomponent nonwoven fibers, J. Mater. Sci. 47 (16) (2012) 5955–5969.
[12] Y.C. Shu, K.J. Hsiao, Thermal behavior and morphological characteristics of cationic dyeable poly(ethylene terephthalate) (CD-PET)/metallocene isotactic polypropylene (m-iPP) conjugated fibers, J. Appl. Polym. Sci. 102 (6) (2006) 5396–5405.
[13] D. Godshall, C. White, G.L. Wilkes, Effect of compatibilizer molecular weight and maleic anhydride content on interfacial adhesion of polypropylene-PA6 bicomponent fibers, J. Appl. Polym. Sci. 80 (2) (2001) 130–141.
[14] F. Ide, A. Hasegawa, Studies on polymer blend of nylon-6 and polypropylene or nylon-6 and polystyrene using reaction of polymer, J. Appl. Polym. Sci. 18 (4) (1974) 963–974.
[15] P.J. Herrerafranco, L.T. Drzal, Comparison of methods for the measurement of fiber matrix adhesion in composites, Composites 23 (1) (1992) 2–27.
[16] A.A. Leal, J.M. Deitzel, S.H. McKnight, J.W. Gillespie, Interfacial behavior of high performance organic fibers, Polymer 50 (5) (2009) 1228–1235.
[17] J.X. Li, A new model for the pull-out of single fibers from low-density polyethylene, Composites 25 (7) (1994) 558–562.
[18] S. Zhandarov, E. Mader, Determination of interfacial parameters in fiber-polymer systems from pull-out test data using a bilinear bond law, Compos. Interfac. 11 (5–6) (2004) 361–391.
[19] L.M. Zhou, Y.W. Mai, C. Baillie, Interfacial debonding and fiber pull-out stresses. 5. A methodology for evaluation of interfacial properties, J. Mater. Sci. 29 (21) (1994) 5541–5550.
[20] M.Q. Tran, K.K.C. Ho, G. Kalinka, M.S.P. Shaffer, A. Bismarck, Carbon fibre reinforced poly(vinylidene fluoride): impact of matrix modification on fibre/polymer adhesion, Compos. Sci. Technol. 68 (7–8) (2008) 1766–1776.
[21] J. Li, F.F. Sun, The effect of maleic anhydride graft on the interfacial adhesion of carbon fiber reinforced thermoplastic polystyrene composite, J. Compos. Mater. 43 (23) (2009) 2717–2725.
[22] A. Gooneie, H. Nazockdast, F. Shahsavan, Effect of selective localization of carbon nanotubes in PA6 dispersed phase of PP/PA6 blends on the morphology evolution with time, part 1: droplet deformation under simple shear flows, Polym. Eng. Sci. 55 (7) (2015) 1504–1519.
[23] C.A. Hieber, H.H. Chiang, Shear-rate-dependence modeling of polymer melt viscosity, Polym. Eng. Sci. 32 (14) (1992) 931–938.
[24] C. Stauffer, The measurement of surface tension by the pendant drop technique, J. Phys. Chem. 69 (6) (1965) 1933–1938.
[25] F.K. Hansen, G. Rodsrud, Surface tension by pendant drop, J. Colloid Interface Sci. 141 (1) (1991) 1–9.
[26] R. Hufenus, F.A. Reifler, K. Maniura-Weber, A. Spierings, M. Zinn, Biodegradable bicomponent fibers from renewable sources: melt-spinning of poly(lactic acid) and poly (3-hydroxybutyrate)-co-(3-hydroxyvalerate), Macromol. Mater. Eng. 297 (1) (2012) 75–84.
[27] G. Desarmot, J.P. Favre, Advances in pull-out testing and data-analysis, Compos. Sci. Technol. 42 (1–3) (1991) 151–187.
[28] C. DiFrancia, T.C. Ward, R.O. Claus, The single-fibre pull-out test .1. Review and interpretation, Compos. Appl. Sci. Manuf. 27 (8) (1996) 597–612.
[29] A.A. Leal, J.C. Veeramachaneni, F.A. Reifler, M. Amberg, D. Stapf, G.A. Barandun, D. Hegemann, R. Hufenus, Novel approach for the development of ultra-light, fully-thermoplastic composites, Mater. Des. 93 (2016) 334–342.
[30] J.C. Moreira, N.R. Demarquette, Influence of temperature, molecular weight, and molecular weight dispersity on the surface tension of PS, PP, and PE. I. Experimental, J. Appl. Polym. Sci. 82 (8) (2001) 1907–1920.
[31] B.D. Favis, J.P. Chalifoux, The effect of viscosity ratio on the morphology of polypropylene/polycarbonate blends during processing, Polym. Eng. Sci. 27 (21) (1987) 1591–1600.
[32] C.Y. Yue, M.Y. Quek, On failure phenomenon in single-fibre pull-out tests, J. Mater. Sci. Lett. 15 (6) (1996) 528–530.
[33] J. Bowling, G.W. Groves, Debonding and pull-out of ductile wires from a brittle matrix, J. Mater. Sci. 14 (2) (1979) 431–442.
[34] G. Mishra, S.L. McArthur, Plasma polymerization of maleic anhydride: just what are the right deposition conditions? Langmuir 26 (12) (2010) 9645–9658.
[35] S. Schiller, J. Hu, A.T.A. Jenkins, R.B. Timmons, F.S. Sanchez-Estrada, W. Knoll, R. Forch, Chemical structure and properties of plasma-polymerized maleic anhydride films, Chem. Mater. 14 (1) (2002) 235–242.
[36] M.R. Piggott, A new model for interface failure in fibre-reinforced polymers, Compos. Sci. Technol. 55 (3) (1995) 269–276.
[37] T.L. Warren, D. Krajcinovic, A fractal model for the static coefficient of friction at the fiber-matrix interface, Composites Part B 27B (1996) 421–430.
[38] K.E. Perepelkin, The effect of the liquid and gas phase transitions on the extrusion stability in man-made fibre and film processes, Fibre Chem. 3 (2) (1972) 115–123.